THE JOURNAL OF BIOLOGICAL CHEMISTRY
Vol. 275, No. 1, Issue of January 7, pp. 343–350, 2000
© 2000 by The American Society for Biochemistry and Molecular Biology, Inc.
Printed in U.S.A.

Mlp2p, A Component of Nuclear Pore Attached Intranuclear Filaments, Associates with Nic96p*

(Received for publication, July 19, 1999, and in revised form, October 27, 1999)

Buket Kosova, Nelly Panté‡, Christiane Rollenhagen‡, Alexandre Podtelejnikov§, Matthias Mann§, Ueli Aebi¶, and Ed Hurt‖

From BZH, Biochemie-Zentrum Heidelberg, Im Neuenheimer Feld 328, D-69120 Heidelberg, Germany

A fraction of the yeast nucleoporin Nic96p is localized at the terminal ring of the nuclear basket. When Nic96p was affinity purified from glutaraldehyde-treated spheroplasts, it was found to be associated with Mlp2p. Mlp2p, together with Mlp1p, are the yeast Tpr homologues, which form the nuclear pore-attached intranuclear filaments (Strambio-de-Castillia, C., Blobel, G., and Rout, M. P. (1999) *J. Cell Biol.* 144, 839–855). Double disruption mutants of *MLP1* and *MLP2* are viable and apparently not impaired in nucleocytoplasmic transport. However, overproduction of *MLP1* causes nuclear accumulation of poly(A)$^+$ RNA in a chromatin-free area of the nucleus.

Nuclear pore complexes are complex structures within the nuclear membrane, which mediate nuclear import and export of transport substrates and shuttling receptors (1). Each nuclear pore complex (NPC)[1] consists of a basic framework (*i.e.* the ring/spoke complex) which exhibits an 8-fold symmetry and spans the double nuclear membrane (2–4). The NPC is attached to peripheral structures such as the short cytoplasmic filaments, the nuclear basket, the nuclear envelope lattice, pore-attached intranuclear filaments, and the nuclear lamina (5–13). Recently, some of these peripheral elements of the NPC gained increased attention since they were proposed to play an important role in the initial docking step of the transport substrate to the pores and the final release from the pores (8, 14–19). In particular, the large nucleoporin Nup358, located at the tips of the short cytoplasmatically attached NPC filaments, is thought to mediate one of the first contacts with transport cargos via the importin/karyopherin α/β complex (15, 19–21). On the other side of the nuclear envelope, release of the import cargo from the nuclear pores appears to occur at the terminal ring of the nuclear basket, and Nup153 might be involved in this final process (16, 18, 22). However, electron microscopy revealed that NPCs do not abruptly end at the nuclear basket, but are connected to a complicated meshwork of intranuclear structures. These structures consist of pore-attached filaments, which deeply penetrate into the nuclear interior or an underlying nuclear envelope lattice (6, 7, 11, 23–26). Therefore, it could be hypothesized that nuclear transport does not end after release of the import cargo from the nuclear basket and followed by intranuclear diffusion, but instead the facilitated transport through the pore could continue on intranuclear "tracks" to distinct intranuclear sites. In a similar way, export cargos may use intranuclear filaments for transport from the nuclear interior to the NPCs. Accordingly, the "gene gating hypothesis" was presented to propose that nuclear pores are connected via intranuclear tracks to distinct locations inside the nucleus (27).

The molecular composition of the intranuclear filamentous system (often referred to as the "nuclear skeleton" or "nuclear matrix"), which has been visualized by a variety of electron microscopy techniques is still poorly characterized (28–36). This is surprising since the nuclear skeleton/nuclear matrix has been assigned many roles in nuclear and chromatin organization, nuclear division, and chromosome segregation, DNA replication and repair, RNA transcription and processing, and intranuclear transport. To date, only the long pore-attached filaments, which deeply penetrate into the nuclear interior and were identified almost 30 years ago by electron microscopy (23), have been characterized on a molecular level. Tpr (for translocated promoter region) was recently shown to be a constituent of these long pore-attached intranuclear fibrils (7, 37, 38). However, it is not completely clear whether Tpr is also located at the short NPC-associated cytoplasmic filaments (5). It was suggested that nuclear pore complex-associated filamentous proteins provide the structural connection between the nuclear interior and the nuclear periphery. However, it is not yet known whether these filaments form channels through which transport occurs, or whether they constitute tracks, along which transport cargos move along (38). Moreover, it was reported that importin/karyopherin β is physically associated with *Xenopus* Tpr (22) and overproduction of Tpr in mammalian cells inhibits poly(A)$^+$ RNA export, but not protein import (39).

Yeast peripheral NPC elements, such as the nuclear basket and the cytoplasmic filaments can be discerned by electron microscopy (40). In the past, we have focussed on various Nsp1p subcomplexes, one consisting of Nsp1p, Nup57p, Nup49p, and Nic96p (41), and another subcomplex between Nsp1p and Nup82p (42), in which Nup159p is also present (43, 44). Recently, Nsp1p and its interacting partners were located by immunoelectron microscopy to distinct sites within the NPC fine structure; accordingly, Nsp1p and Nic96p exhibit a dual location on both sides of the central gated channel, and at the terminal ring of the nuclear basket (40). Thus, the fraction of

* This work was supported in part by grants from the Human Frontiers Science Program (HFSP) (to U. A. and E. C. H.), the M. E. Müller Foundation of Switzerland, and the Swiss National Science Foundation (to N. P.). The costs of publication of this article were defrayed in part by the payment of page charges. This article must therefore be hereby marked "*advertisement*" in accordance with 18 U.S.C. Section 1734 solely to indicate this fact.

‡ Present address: Institute of Biochemistry, Swiss Federal Institute of Technology (ETH), Universitätsstr. 16, CH-8092 Zürich, Switzerland.

§ Present address: CEBI Odense University, Staermosegaardsvej 16, DK-5230 Odense, Denmark.

¶ Present address: M. E. Müller Institute for Microscopy, Biozentrum, University of Basel, CH-4056 Basel, Switzerland.

‖ Recipient of Deutsche Forschungsgemeinschaft Grant SFB352. To whom all correspondence should be addressed. Tel.: 49-6221-54-41-73; Fax: 49-6221-54-43-69; E-mail: cg5@ix.urz.uni-heidelberg.de.

[1] The abbreviations used are: NPC, nuclear pore complex; PCR, polymerase chain reaction; UTR, untranslated region; GST, glutathione *S*-transferase; PAGE, polyacrylamide gel electorphoresis.

TABLE I
Yeast strains

Strain	Genotype
RS453	MATa/α,ade2/ade2,his3/his3,leu2/leu2,trp1/trp1,ura3/ura3
ProtA-NIC96	MATa,ade2,his3,leu2,trp1,ura3,URA3-ProtA-NIC96
SEH1-ProtA	MATa or α,ade2,his3,leu2,trp1,ura3,seh1::HIS3 (pRS316-SEH1-ProtA)
mlp2$^-$	MATa or α,ade2,his3,leu2,trp1,ura3,mlp2::HIS3
mlp1$^-$	MATa or α,leu2,lys2,ura3,mlp1::LEU2
mlp1$^-$/mlp2$^-$	MATa or α,ade2,his3,leu2,ura3,mlp1::LEU2,mlp2::HIS3
nup133$^-$	MATa or α,ade2,his3,leu2,trp1,ura3,nup133::HIS3
MLP2-ProtA::HIS3	MATa or α,ade2,his3,leu2,trp1,ura3,MLP2-ProtA::HIS3
MLP2-GFP::HIS3	MAT α,ade2,his3,leu2,trp1,ura3,MLP2-GFP::HIS3 (pASZ11)
mlp2$^-$/nup133$^-$	MATa or α,ade2,his3,leu2,trp1,ura3,nup133::HIS3,mlp2::HIS3 (pHT4467-MLP2-GFP::HIS3,pASZ11)
MLP1-TEV-ProtA	MATa or α,leu2,lys2,ura3,mlp1::LEU2 (YEp420-MLP1-TEV-ProtA)
mlp1$^-$/nup133$^-$	MATa or α,ade2,his3,leu2,trp1,ura3,nup133::HIS3,mlp1::LEU2 (YCplac33-MLP1-GFP,pASZ11)

Nic96p, which is located at the terminal ring, could directly contact to pore-attached intranuclear filaments.

To identify additional Nic96p-interacting proteins in yeast, we treated yeast spheroplasts with glutaraldehyde prior to affinity purification. This allowed us to identify Mlp2p, which associates with protein A-tagged Nic96p (ProtA-Nic96p). Mlp2p is highly homologous to Mlp1p, a previously identified myosin-like protein in yeast (45). Both Mlp1p and Mlp2p are the two closest homologues of the higher eukaryotic Tpr proteins which form NPC-attached intranuclear filaments.

EXPERIMENTAL PROCEDURES

Yeast Strains and Plasmids—The yeast strains used in this study are listed in Table I. Cells were grown in minimal SDC or rich YPD medium. Genetic manipulations of yeast were performed as described (46). The following yeast plasmids were used: pHT4467, *ARS*/*CEN* plasmid with the *URA3* and *ADE3* marker; pUN100, pRS314, pRS316, YCplac33, and pASZ11, *ARS*/*CEN* plasmids with the *LEU2*, *URA3,* and *ADE2* marker, respectively. pRS424 and YEplac112, 2 μ plasmids with the *TRP1* marker. pRS426, YEp352, and YEp420, 2-μm plasmids with the *URA3* marker. pRS425, 2-μm plasmid with the *LEU2* marker. Manipulation and analysis of DNA such as restriction analysis, end-filling, ligations, DNA sequencing, and PCR amplifications were performed according to Ref. 47. Gene disruptions were made by the one-step disruption method (48).

Plasmid Constructions and Gene Disruptions—Construction of strains with integrated *MLP2* constructs was done as follows: by PCR, a *Not*I site was generated at the stop codon. This yielded plasmid YEplac112-MLP2-C (*Not*I). The genes encoding ProtA and GFP, each available as *Not*I restriction fragment, were inserted into the corresponding *Not*I site within YEplac112-MLP2-C (*Not*I). The unique *Spe*I site within the 3′-UTR of *MLP2* was used for the blunt end insertion of the *HIS3* gene. For integration of tagged *MLP2-ProtA::HIS3* and *MLP2-GFP::HIS3*, the plasmids were cut with convenient restriction enzymes to release the integration fragments. The RS453 diploid strain was transformed with these linearized DNA fragments and colonies that grew on SDC-His plates were selected. After sporulation on YPA plates and tetrad analysis, haploid progeny, which contained the correct integration were selected. Integrations were verified by PCR analysis. Whole cell extracts from these strains were prepared and analyzed for the expression of the GFP- and ProtA-tagged Mlp2p by Western blotting using anti-GFP and anti-ProtA antibodies, respectively. For the disruption of the entire *MLP2* ORF, a linear *mlp2::HIS3* fragment was generated and used to transform the RS453 diploid strain. Colonies that grew on SDC-His plates and showed the correct integration (as verified by PCR Southern analysis) were sporulated on YPA. Tetrad analysis showed a 4:0 segregation for cell viability on YPD plates, and a 2:2 segregation of the *HIS3* marker. To recover the full-length *MLP2* gene from the chromosome, the "GAP-repair" method was used. To do so, the joined 5′- and 3′-UTR fragments of *MLP2* (derived from pUN100-mlp2Δ) were inserted into high copy number plasmids pRS424 and pRS426. For gap repair, these constructs were digested with *Not*I/*Spe*I, releasing an internal 0.1-kilobase fragment. The gel-purified pRS424–5′/3′-UTR-MLP2 and pRS426–5′/3′-UTR-MLP2 fragments were transformed into a haploid RS453 strain carrying integrated *MLP2-GFP::HIS3*. Colonies were selected on SDC-Trp or SDC-Ura plates, respectively. Transformants were screened for an increased GFP signal in the fluorescence microscope, which allowed identification of colonies which contained pRS424-MLP2-GFP and pRS426-MLP2-GFP, respectively. GST-tagged Mlp2p-C constructs were made by PCR from genomic DNA and cloned into pGEX-4T-3 (Amersham Pharmacia Biotech). For expression of GFP-tagged Mlp2p-C constructs in yeast, PCR-derived DNA was cloned into pRS425-P_{NOP1}-GFP. For tagging of the *MLP1* gene, a *Not*I restriction site was generated by PCR immediately before the stop codon to yield YEp420-MLP1. The generated *Not*I site of YEp420-MLP1 (*Not*I) was used to insert ProtA, TEV-ProtA, and GFP, as *Not*I cassettes as described above. To generate GFP-tagged Mlp1p-C (residue 1446–1875), the last 429 amino acids from Mlp1p were amplified by PCR from genomic DNA and cloned into pRS425-P_{NOP1}-GFP.

Affinity Purification of Nic96p and Seh1p—Affinity purification of ProtA-Nic96p and Seh1p-ProtA from yeast spheroplasts treated with 0.1% glutaraldehyde was done as follows: a yeast strain expressing ProtA-NIC96 (41) was grown in 2 liters of SDC-Leu medium for 14 h at 30 °C to an $A_{600\ nm}$ of 1. Cells were collected by centrifugation, spheroplasted with 5 mg of 20T Zymolyase/g of cells, resuspended in 100 ml of sorbitol buffer (1.2 M sorbitol, 0.02 M KP_i, pH 7.4), and split into four 25-ml aliquots. Increasing concentrations of glutaraldehyde were added: 0, 0.01, 0.1, and 1% and it was incubated for 30 min on ice. After two washing steps with sorbitol buffer, ProtA-Nic96p affinity purification on IgG-Sepharose beads was done as described previously (49).

Mass Spectrometry—Mass spectrometry of bands excised from SDS-polyacrylamide gels was done as described elsewhere (50). Tryptic peptide mixtures obtained as a result of in-gel digestion were analyzed on a matrix-assisted laser desorption time of flight mass spectrometer (REFLEX III, Bruker-Daltonics, Bremen, Germany). Matrix and samples were prepared as described (51). Proteins were identified via non-redundant protein sequence data base search with a list of detected tryptic peptides using PeptideSearch software.

Purification of Karyopherin α and β and GST-Mlp2p-C from Escherichia coli and Solution Binding Assay—Expression and purification of recombinant karyopherin α and β, and purification of thrombin-cleaved proteins were done as outlined by Ref. 52. Construction of recombinant GST-Mlp2p-C (COOH-terminal domain ranging from residues 1500–1679), GST-Mlp2-C-NLS, and GST-Mlp2-C-FSFG was done by PCR and the fusion constructs were inserted into the *E. coli* expression plasmid pGEX-4T-3 vector (Amersham Pharmacia Biotech). Induction of GST alone or GST-tagged fusion proteins and their subsequent purification on glutathione-Sepharose beads was done as described (53). After washing with universal buffer, purified karyopherin α (~2 μg) and karyopherin β (~2 μg), either as single subunits or complex, were mixed in 100 μl of buffer with GST beads or GST fusion protein beads. After incubating at 4 °C for 1 h, columns were washed and the bound proteins were eluted by SDS sample buffer. Bound and unbound fractions were analyzed by SDS-PAGE and Coomassie/silver staining, or Western blotting using the anti-Kap60p and Kap95p antibodies.

Fluorescence Microscopy—To detect GFP *in vivo*, the GFP signal was analyzed in the fluorescein channel of a Zeiss Axioskop fluorescence microscope. Pictures were taken with a Xillix Microimager CCD camera and digital pictures processed by the software program Openlab (Improvision, Coventry, United Kingdom).

Yeast Survival Analysis after UV Irradiation—UV light sensitivity of *mlp1*$^-$, *mlp2*$^-$, and *mlp1*$^-$/*mlp2*$^-$ mutants was analyzed by diluting freshly growing yeast strains in YPD medium and spotting equivalent amounts of cells (diluted in 10^{-1} steps) onto YPD plates. The plates were UV-irradiated (Stratalinker UV cross-linker/254 nm UV light bulbs; model 1800) with an intensity from 0 to 150,000 μJ/cm^2 and plates were incubated for 3 days at 30 °C.

Electron Microscopy—Glycerol spraying/low-angle rotary metal shadowing of the purified Mlp1p was performed as described (54).

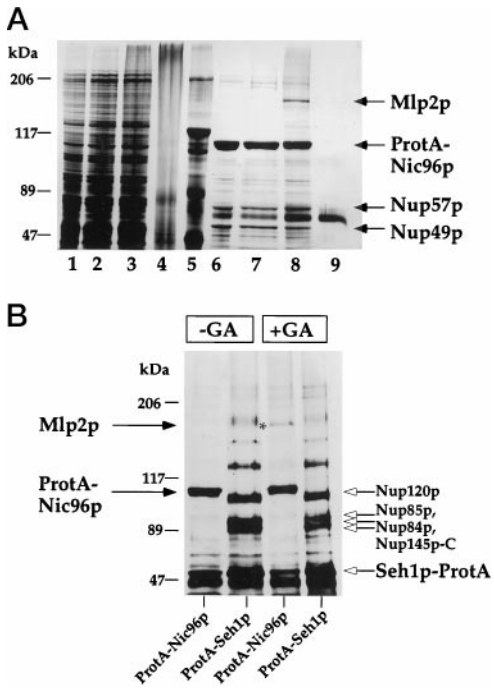

FIG. 1. **Purification of ProtA-Nic96p from glutaraldehyde-treated cells reveals interaction with the yeast Tpr-like protein Mlp2p.** *A,* purification of ProtA-Nic96p from yeast spheroplasts which were incubated with different concentrations of glutaraldehyde. 25 μl of whole cell extracts (*lanes 1–4*) and derived ProtA-Nic96p eluates (*lanes 6–9*) were analyzed by SDS-PAGE followed by silver staining. *1* and *6*, no glutaraldehyde; *2* and *7*, 0.01% glutaraldehyde; *3* and *8*, 0.1% glutaraldehyde; *4* and *9*, 1% glutaraldehyde; *5*, high molecular mass protein standard (kDa). The 160-kDa band which co-purified with ProtA-Nic96p was identified by mass spectrometry to be yeast ORF YIL149c (Mlp2p). *B,* purification of ProtA-Nic96p and Seh1p-ProtA, respectively, from yeast spheroplasts which were incubated with no (*−GA*) and with 0.1% glutaraldehyde (*+GA*) prior to isolation. 25 μl of ProtA-Nic96p and Seh1p-ProtA eluates were analyzed by SDS-PAGE and silver staining. Indicated are Mlp2p (also by an *asterisk* within the gel) and ProtA-Nic96p (*filled arrows*), and the subunits of the Nup84p complex including Seh1p-ProtA (*open arrows*).

Embedding, thin sectioning, and immuno-gold labeling of cells expressing Mlp2p-ProtA and Mlp1p-ProtA was performed according to Ref. 40 with one modification: the Mlp2p-ProtA and Mlp1p-ProtA spheroplasts were extracted with 0.02% Triton X-100 before labeling with the anti-protein A antibody directly conjugated to colloidal gold.

Miscellaneous—SDS-polyacrylamide gel electrophoresis, Western blotting, indirect immunofluorescence, and analysis of poly(A)$^+$ RNA export were performed as described earlier (55).

RESULTS

Purification of Nic96p from Glutaraldehyde-fixed Spheroplasts Reveals an Association with Mlp2p Which Is Homologous to the Vertebrate Tpr Proteins—Affinity purification of ProtA-Nic96p from yeast spheroplasts has shown an interaction with Nsp1p, Nup49p, and Nup57p (41). To find components that associate less strongly with Nic96p, we treated yeast spheroplasts with glutaraldehyde (to stabilize/cross-link protein complexes) prior to affinity purification of ProtA-Nic96p. Interestingly, the ProtA-Nic96p eluate derived from the lysate treated with 0.1%, but not 0.01% glutaraldehyde revealed, besides Nup49p, Nup57p, and Nsp1p, an additional band of about 160 kDa on the silver-stained SDS-polyacrylamide gel (Fig. 1*A, lane 8*). The 160-kDa band was excised from the gel, in-gel digested with trypsin, and analyzed by matrix-associated laser desorption ionization mass spectrometry, followed by a data base search on the detected peptide masses. In total, 21 peptides from this band were detected which corresponded to a 15% protein sequence coverage. According to our general criteria (51), this sequence coverage and mass accuracy was good enough for the unambiguous identification of this band which corresponds to the yeast ORF YIL149c, which has a predicted molecular mass of 195 kDa. In the course of this work, Blobel and colleagues (56) identified and characterized this ORF and called it Mlp2p, one of the two yeast Tpr homologues. Mlp2p is homologous to yeast Mlp1p (myosin-like protein), which was found earlier as a 218-kDa coiled-coil protein (45). As deduced from the amino acid sequence, Mlp2p (as well as Mlp1 and other Tpr proteins) can be divided into two distinct domains: an amino-terminal domain of roughly 1500 amino acids, which has numerous heptad repeats with the potential to form α-helical coiled-coil structures (56) and a short carboxyl-terminal domain of roughly 180 amino acids, which is devoid of heptad repeats, but exhibits one F*X*FG motif typically found in repeat sequence containing nucleoporins such as Nsp1p and Nup1p, and a putative bipartite basic NLS (see also later). To show that Mlp2p is specifically associated with Nic96p under conditions of glutaraldehyde fixation, another nucleoporin, Seh1p-ProtA, which is organized with five other components in the Nup84p complex (57), was affinity purified under similar conditions from spheroplasts, treated with 0.1% glutaraldehyde. When the two different ProtA-fusion protein preparations were compared by SDS-PAGE and silver staining, the 160-kDa band corresponding to Mlp2p is only seen in the ProtA-Nic96p, but not Seh1p-ProtA eluate (Fig. 1*B*). This shows that Mlp2p specifically associates with Nic96p under the chosen conditions of glutaraldehyde treatment.

Mlp2p and Mlp1p Are Nuclear Pore-associated Proteins—To determine its intracellular location, Mlp2p was tagged with GFP at its carboxyl-terminal end and the construct was integrated at the authentic gene locus to replace endogenous *MLP2* by *MLP2-GFP*. Mlp2p-GFP gave a distinct nuclear envelope labeling which was punctate and often excluded from the area in which the nuclear membrane is adjacent to the vacuole (Fig. 2*A*). This staining is typical for a NPC distribution in yeast and suggests that Mlp2p is restricted to the part of nuclear envelope which also contains nuclear pores. This conclusion is further supported by the finding that Mlp2p-GFP co-clusters with nuclear pores in *nup133*$^-$ cells (Fig. 2*A*; see also Ref. 58). However, a residual intranuclear staining also becomes visible under these conditions. Accordingly, Mlp2p is nuclear pore-associated, but it is also found inside the nucleus. Since Mlp1p is highly homologous to Mlp2p, Mlp1p was also tagged with GFP and its subcellular location was determined by fluorescence microscopy. Similar to Mlp2p, Mlp1p shows a nuclear pore distribution in yeast (Fig. 2*B*). This result is in contrast to a previous finding, in which Mlp1p was located to dot-like structures adjacent to the nucleus by indirect immunofluorescence microscopy (45). However, in this case Mlp1p was overproduced, whereas here the GFP-tagged *MLP1* was expressed under its authentic promoter and inserted into a low copy *ARS*/*CEN* plasmid. To test whether overproduced Mlp1p-GFP and Mlp2p-GFP form aggregates, both fusion genes were inserted into high copy number plasmids and expressed in yeast. Overproduction of Mlp2p-GFP or Mlp1p-GFP caused the appearance of an extremely bright fluorescent spot, often close to the nuclear envelope (data not shown). This suggests that overproduction causes aggregate formation of both Mlp2p and Mlp1p (see also Ref. 56). Since it is possible that Mlp2p and Mlp1p form a coiled-coil heterodimer, we overexpressed both proteins in yeast. However, the same GFP aggregates formed under the condition of co-overproduction (data not shown).

To determine the localization of Mlp1p and Mlp2p on the ultrastructural level, strains expressing Mlp1p-ProtA and Mlp2p-ProtA, respectively, were prepared by pre-embedding

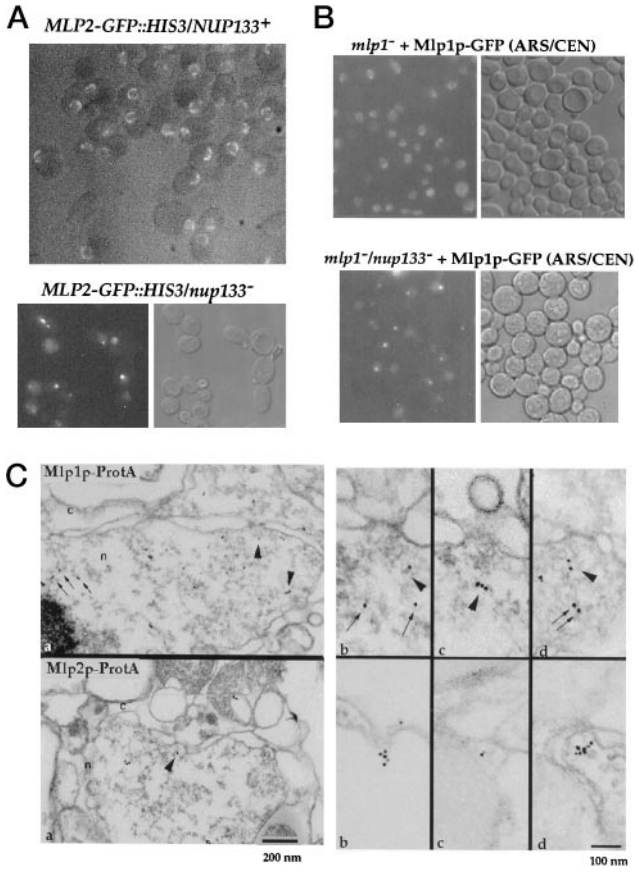

FIG. 2. **Mlp1p and Mlp2p are NPC-associated proteins.** Nuclear envelope and nuclear pore location of Mlp2p-GFP (*A*) and Mlp1p-GFP (*B*). A haploid double mutant *MLP2-GFP::HIS3/nup133::HIS3* was generated. Mlp1p-GFP was expressed from a single copy plasmid (*ARS/CEN*) transformed into the *mlp1*$^-$ single or *mlp1*$^-$/*nup133*$^-$ double disrupted strain. Shown are fluorescence and Nomarski pictures. In the case of *MLP2-GFP::HIS3* cells (*upper panel* in *A*), the fluorescence and Nomarski pictures were merged. *C,* immunoelectron microscopy localization of Mlp1p and Mlp2p. *a,* overview of nuclei cross-sections of Mlp1p-ProtA and Mlp2p-ProtA pre-embedding labeled with anti-ProtA antibody directly conjugated to 8-nm colloidal gold particles. *b-d,* a gallery of selected examples of gold-labeled nuclear pore cross-sections from Mlp1p-ProtA and Mlp2p-ProtA strains. Mlp2p was located at the nuclear periphery of the pore (at 51 ± 10 nm from the central plane of the pore), whereas Mlp1p was found associated with pore-attached filaments at two distinct locations: at 90 ± 20 nm (*arrowheads*) and 180 ± 38 nm (*arrows*) from the central plane of the pore. *c*, cytoplasm; *n*, nucleus. *Scale bars* correspond to 200 (*a*) and 100 (*b-d*) nm.

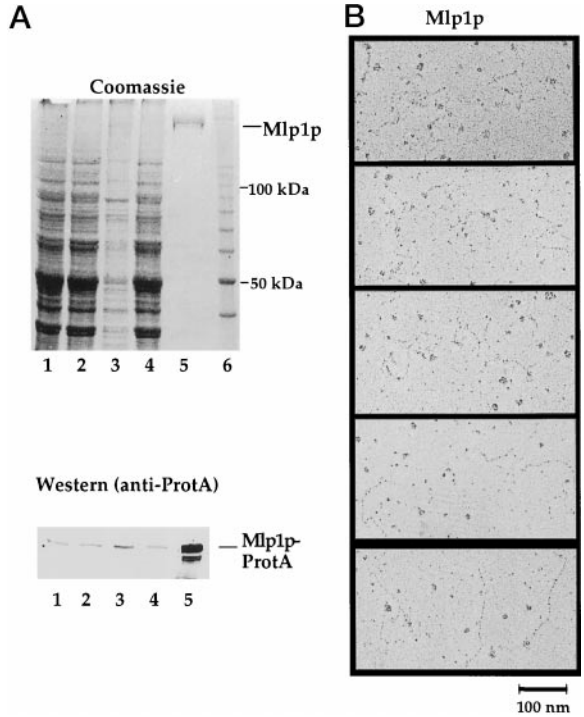

FIG. 3. **Purification and structure of Mlp1p.** *A,* affinity purification of Mlp1p-TEV-ProtA by IgG-Sepharose chromatography and cleavage by the TEV protease, or acetic acid elution, was performed as described under "Experimental Procedures." A cell homogenate (*1*), soluble supernatant (*2*), insoluble pellet (*3*), flow-through (*4*), and a 200-fold equivalent of the TEV-cleaved and eluted Mlp1p (*5*) were analyzed by SDS-8% PAGE, followed by Coomassie staining and Western blotting, using anti-ProtA antibodies. A protein standard, *i.e.* 10-kDa ladder with a stronger 50-kDa band, is also shown (*6*). The position of Mlp1p is indicated. In the case of Western blot analysis, Mplp1-ProtA was not cleaved by TEV, but eluted from the IgG-Sepharose column by acetic acid. *B,* electron microscopic appearance of purified yeast Mlp1p after glycerol spraying/low-angle rotary metal shadowing. A gallery of long, mostly curved filamentous molecules with a tendency to anneal head to tail (see *last panel down*) is displayed. The *scale bar* represents 100 nm.

immunoelectron microscopy using a colloidal gold-conjugated anti-ProtA antibody (40). As shown in Fig. 2*C*, the anti-ProtA antibody labeled the nuclear periphery of the nuclear pores of both ProtA-tagged Mlp1p and Mlp2p. For Mlp2-ProtA, gold particles were located at 51 ± 10 nm (mean ± S.D., $n = 15$) from the central plane of the pore. Gold particles were also found in the nucleus. However, the number of nuclear gold particles significantly varied from cell to cell (going from 0 to 30% of the total gold particles), and their distribution seemed to be random with an unclear association with closest pores. In contrast to Mlp2p, most of the gold particles for Mlp1p-ProtA were found in the nucleus (60% nuclear, 38% at the pores, and 2% cytoplasmic). For the gold particles associated with pores, two distinct locations were found, one at 90 ± 20 nm (mean ± S.D., $n = 15$; see Fig. 2*C, arrowheads*) and the other at 180 ± 38 nm (mean ± S.D., $n = 15$; see Fig. 2*C, arrows*) from the central plane of the pore. In both cases, the gold particles were often aligned on tracks and seemed to be associated with pore-attached filaments (see Fig. 2*C*).

ProtA-tagged Mlp2p and Mlp1p (containing the TEV proteolytic cleavage site) were affinity purified under standard conditions previously used to purify bona fide nucleoporins (58). The Coomassie-stained SDS-polyacrylamide gel showed basically a single band with a good yield for the purification of Mlplp after TEV cleavage (Fig. 3*A*). When Mlp2p-ProtA was affinity purified, full-length Mlp2p-ProtA was clearly visible, but the yield was lower as compared with Mlp1p and the preparation was less pure (data not shown). Western blot analysis of the Mlp2p-ProtA and Mlp1p-ProtA eluates did not show co-enrichment of Nic96p (data not shown). To test for heterodimer formation, purified Mlp2p-ProtA was blotted onto nitrocellulose and probed with affinity purified anti-Mlp1p antibodies; however, no Mlp1p was detected in the purified Mlp2p-ProtA fraction (data not shown). This shows that under conditions used to purify subcomplexes of the NPC (*e.g.* Nsp1p or Nup84p complex), Mlp2p and Mlp1p predominantly purify as single components.

We analyzed the structure of purified Mlp1p by electron microscopy after glycerol spraying/low-angle rotary metal shadowing (54). Although the isolated Mlp1p was more than 95% pure, as judged from the SDS-polyacrylamide gel, the sample yielded a rather heterogeneous morphology in the electron microscope. Nevertheless, about 10% of the particles appeared as long, thin and mostly curved filamentous molecules (Fig. 3*B*). In a control, another yeast ProtA-tagged nucleoporin (ProtA-Nup85p) was affinity purified and prepared for glycerol

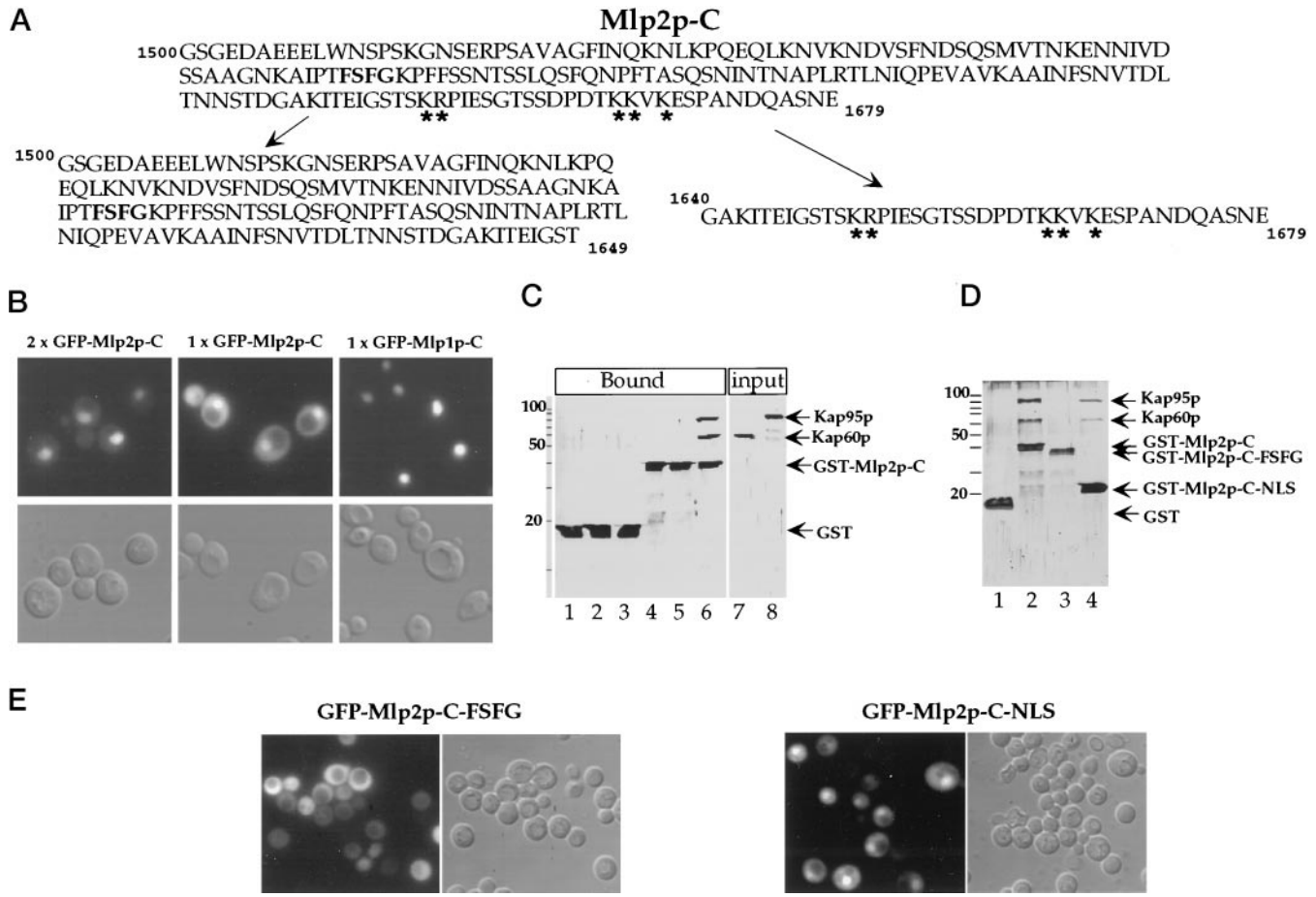

FIG. 4. **The C-domain of Mlp2p has nuclear targeting activity and interacts with the karyopherin α/β complex.** *A,* the carboxyl-terminal domain of Mlp2p contains a putative bipartite NLS and a FSFG motif typically found in F*X*FG repeat sequences containing nucleoporins. Shown is the Mlp2p sequence from residue 1500–1679. Indicated in *bold* is the FSFG motif, and *asterisks* indicate lysine and arginines within a putative NLS. *B,* the C-domains of Mlp2p (residues 1500–1679) and Mlp1p (residue 1446–1875) can target GFP into the nucleus. The subcellular location of the corresponding GFP fusion proteins was analyzed by fluorescence microscopy; cells were also viewed by Nomarski optics. *C,* the C-domain of Mlp2p binds *in vitro* to the karyopherin α/β complex. GST or GST-Mlp2p-C were purified by affinity chromatography. Beads with immobilized GST or GST-Mlp2p were incubated with *E. coli* purified yeast karyopherin α (Kap60p) and karyopherin β (Kap95p), or both together. The bound fractions 1–6 were analyzed by SDS-PAGE and silver staining. *1* and *4*, Kap60p; *2* and *5*, Kap95p; *3* and *6*, Kap60p mixed with Kap95p; *7*, input Kap60p; *8*, input Kap95p. The positions of GST, GST-tagged Mlp2p-C, Kap60p, and Kap95p are indicated. *D,* the putative bipartite NLS within of Mlp2p-C binds *in vitro* to karyopherin α/β. GST, GST-Mlp2p-C-NLS, and GST-Mlp2p-C-FSFG were purified by affinity chromatography and incubated with karyopherin α/β. Shown are the bound fractions. *1*, GST incubated with karyopherin α/β; *2*, GST-Mlp2p-C incubated with karyopherin α/β; *3*, GST-Mlp2p-C-FSFG (residue 1500–1649) incubated with karyopherin α/β; *4*, GST-Mlp2p-C-NLS (residue 1640–1679) incubated with karyopherin α/β. *E,* the putative bipartite NLS of Mlp2p-C (residues 1640–1679) can target GFP into the nucleus. The subcellular location of the corresponding GFP-fusion proteins, GFP-Mlp2p-C-NLS and GFP-Mlp2p-C-FSFG, were analyzed by fluorescence microscopy.

spraying/low-angle rotary metal shadowing under identical conditions, but no thin and filamentous structures were seen in the electron microscope.[2]

A Short Sequence within C-domain of Mlp2p Binds in Vitro to the Karyopherin α/β—Since both GFP-tagged Mlp2p and Mlp1p exhibit, besides a distinct nuclear envelope location, an intranuclear staining (see also Fig. 2), it is possible that they are imported into the nucleus with the help of an NLS. It was found recently that the C-domain, but not the coiled-coil N-domain of mammalian Tpr, contains a nuclear localization signal (39, 59). According to these findings, we tested whether the C-domains of Mlp2p (see also Fig. 4*A* for sequence) and Mlp1p exhibit a nuclear localization sequence which can target an attached reporter protein into the nucleus. Therefore, the C-domains of Mlp2p and Mlp1p were fused to GFP and the *in vivo* location of the corresponding fusion proteins was determined by fluorescence microscopy (Fig. 4*B*). This revealed that both Mlp2p-C and Mlp1p-C domains can mediate efficient transport of GFP into the nucleus. GFP alone does not accumulate inside the nucleus (60). Although both GFP fusion proteins are strongly concentrated inside the nucleus, GFP-Mlp2p-C, but not GFP-Mlp1p-C, was also detected in the cytoplasm. Since GFP-Mlp2p-C has a calculated molecular mass of ~40 kDa, it may not be efficiently retained inside the nucleus due to diffusion back into the cytoplasm. In contrast, GFP-Mlp1p-C is larger (~60 kDa) and therefore may be better retained inside the nucleus. We therefore made a 2× GFP-Mlp2p-C construct and expressed it in yeast. The extent of nuclear accumulation of 2× GFP-Mlp2p-C increased and the cytoplasmic signal decreased. However, a small cytoplasmic signal was still visible (Fig. 4*B*). This could suggest that the NLS of Mlp2p is less strong as compared with the Mlp1p-NLS. In conclusion, the C-domains of Mlp2p and Mlp1p contain NLSs which most likely target the corresponding full-length proteins into the nucleus.

The COOH-terminal domain of Mlp2p contains a sequence which resembles a bipartite NLS; in addition, this domain also exhibits one F*X*FG motif typically found in repeat sequences containing nucleoporins such as Nsp1p, Nup1p, and Nup2p (Fig. 4*A*). We therefore tested whether the C-domain of Mlp2p

[2] U. Aebi, unpublished results.

can interact with karyopherin α, karyopherin β, or both. The last 180 amino acids from Mlp2p were fused to the GST protein and GST-Mlp2p-C was expressed in *E. coli*. After purification by glutathione affinity chromatography, recombinant and purified karyopherin α (Kap60p) and karyopherin β (Kap95p) were added separately or as a reconstituted complex to the immobilized GST-Mlp2p-C (Fig. 4*C*). Kap60p or Kap95p monomers did not significantly bind to GST-Mlp2p-C; in contrast, a strong and cooperative binding of the Kap60p·Kap95p complex to GST-Mlp2p-C beads was observed (Fig. 4*C*). The immobilized GST alone served as a negative control, to which no binding of the karyopherin α/β complex could be detected (Fig. 4*C*). It was recently shown that the karyopherin α/β complex cooperatively binds to F*X*FG, but not GLFG repeat sequences-containing nucleoporins (52). This could suggest that the C-domain of Mlp2p binds via its F*X*FG containing sequence or via a NLS to karyopherin α/β. We therefore separated the sequence containing the FSFG motif (residue 1500–1649) from the putative bipartite NLS (residue 1640–1679) and fused both domains to GST. Whereas GST-Mlp2p-C-FSFG no longer bound to karyopherin α/β, the GST-Mlp2p-C-NLS fusion construct retained karyopherin α/β binding activity (Fig. 4*D*). This shows that the putative bipartite NLS within Mlp2p-C can interact with karyopherin α/β. Finally, this bipartite-type NLS was fused to GFP and expressed in yeast. This revealed that the NLS-like sequence, but not the FSFG-containing part, exhibits nuclear targeting activity (Fig. 4*E*).

The mlp1⁻/mlp2⁻ Double Mutant Is Viable, but Shows an Increased Sensitivity to UV Light—To study the *in vivo* role of Mlp2p and to find out whether it functionally overlaps with Mlp1p, the complete *MLP2* ORF was replaced by the *HIS3* gene in a diploid yeast strain (see "Experimental Procedures"). After sporulation of the heterozygous *mlp2::HIS3/MLP2* diploid strain and tetrad analysis, four viable spores were recovered, of which the two *mlp2::HIS3* containing progeny (further designated as *mlp2⁻*) grew similar as compared with the *MLP2⁺* progeny (data not shown). Since Mlp1p may compensate for the loss of the Mlp2p function, a haploid double disruptant was generated by mating and tetrad analysis. This *mlp1⁻/mlp2⁻* strain was still viable and no clear growth defect was noticed at the various tested temperatures as compared with *MLP1⁺/MLP2⁺* progeny. However, a dot-spot growth analysis revealed that the double disrupted strain forms heterogeneous colonies (Fig. 5). In addition to colonies of normal size, smaller colonies also became visible in *mlp1⁻/mlp2⁻* mutants. This shows that the two yeast Tpr-like proteins are required for optimal cell growth. Since *mlp1* mutants were shown to have an increased sensitivity to UV light (45), and the observed heterogeneous colony size in the double mutant would be consistent with a defect in DNA repair, we analyzed whether the *mlp1⁻/mlp2⁻* null mutants are hypersensitive to UV light causing DNA damage (61). Indeed, the *mlp1⁻/mlp2⁻* double disrupted strain displayed a significantly increased sensitivity to ultraviolet radiation (Fig. 5), whereas the single disrupted *mlp1⁻* and *mlp2⁻* strains were less sensitive to this treatment (Fig. 5). Thus, the *mlp1⁻/mlp2⁻* double mutant is vulnerable to DNA damaging methods such as UV light irradiation (see also "Discussion").

Poly(A)⁺ RNA Export Is Inhibited in Mlp1p-overproducing Cells—To find out whether nucleocytoplasmic transport is affected in the *mlp2* or *mlp1* disruption mutants, nuclear protein import of Npl3p-GFP and NLS-GFP-lacZ, and mRNA export were analyzed. No apparent defect in nuclear import and export was observed in neither the single nor the double disrupted strains (data not shown). However, overproduction of Mlp1p (achieved by transforming a haploid RS453 wild-type strain with a high-copy number plasmid containing *MLP1*) caused nuclear accumulation of mRNA (Fig. 6*A*). In contrast, overproduction of *MLP2-GFP* did not reveal such impairment, whereas overexpression of both *MLP1* and *MLP2-GFP* enhanced the inhibition of poly(A)⁺ RNA export. We noticed that the poly(A)⁺ RNA signal which accumulated in Mlp1p-overproducing cells did not coincide with the DNA staining. To find out in which part of the nucleus the mRNA accumulated, indirect immunofluorescence was performed using anti-Nsp1p (Fig. 6*B*) and anti-Nop1p antibodies (Fig. 6*C*). Clearly, the bright poly(A)⁺ RNA spot seen in Mlp1p-overproducing cells is confined within the nucleus, in an area which is devoid of chromatin, but is not the nucleolus (Fig. 6, *B* and *C*, see also "Discussion").

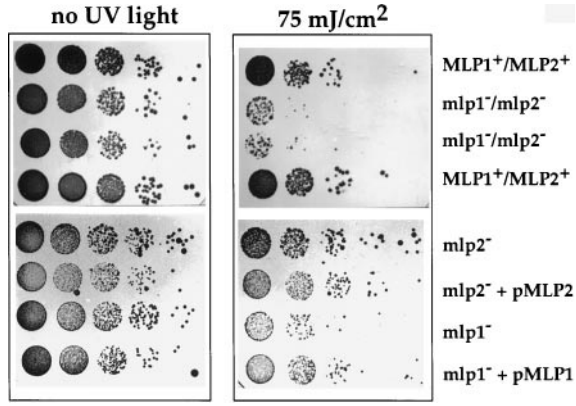

FIG. 5. **The *mlp1⁻/mlp2⁻* double disruption mutant is viable, but exhibits an increased sensitivity to UV light.** The same amount of cells derived from the four spores of a complete tetrad (strains *MLP1⁺/MLP2⁺* or *mlp1⁻/mlp2⁻*), and from *mlp1⁻* and *mlp2⁻* single disrupted strains which were also complemented by plasmid-borne *MLP1* and *MPL2*, respectively, were diluted in 10^{-1} steps, spotted onto YPD plates, and exposed to the indicated doses of UV light. It was grown for 4 days at 30 °C in the dark.

DISCUSSION

Nucleocytoplasmic trafficking through the nuclear pore complexes is a bidirectional process. However, it is not known whether guided transport continues after translocation through the pore channel on NPC-attached intranuclear and cytoplasmic filaments. During nuclear protein import, termination of transport was suggested to occur at the nuclear basket (*i.e.* the terminal ring) in *Xenopus* oocyte nuclei (16), but *in vivo* facilitated transport of certain import cargos may continue from the nuclear pores to distinct intranuclear sites (for discussion see Ref. 60). Conversely, intranuclear transport of export cargoes (*e.g.* mRNPs) may also be facilitated by guided transport on track-like structures.

Intranuclear filaments, which are attached to the inner site of nuclear pore complexes could play a role in facilitated intranuclear transport steps, either by serving as tracks or forming intranuclear channels. It is now clear that Tpr proteins are constituents of the NPC-attached intranuclear filaments. Our work shows that the yeast Tpr protein, Mlp2p, physically associates with Nic96p (or a member of the Nic96p complex). Although this interaction was found when spheroplasts were treated with glutaraldehyde prior to affinity purification of ProtA-Nic96p, it seems that Mlp2p was not covalently cross-linked to Nic96p; the apparent molecular mass of the putative cross-link product on SDS-PAGE (~160 kDa) does not match with the calculated molecular mass (~300 kDa). How glutaraldehyde fixation allows a better co-enrichment of Mlp2p during ProtA-Nic69p purification is not clear. However, Mlp2p does not unspecifically co-purifiy with any nucleoporin during purification from glutaraldehyde-treated spheroplasts as a

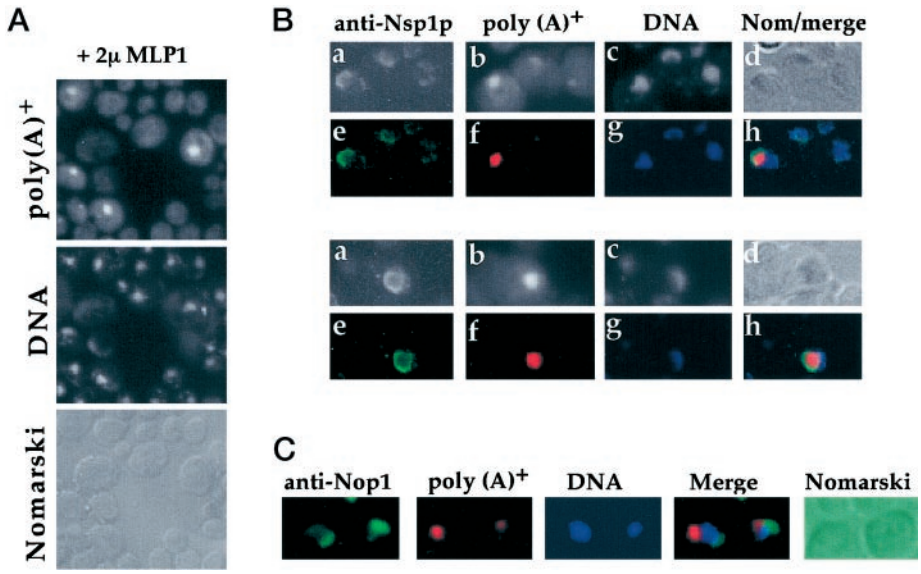

FIG. 6. **Overproduction of Mlp1p causes intranuclear poly(A)$^+$ RNA accumulation.** *In situ* poly(A)$^+$ RNA hybridization (*A*) combined with anti-Nsp1p (*B*) and anti-Nop1p (*C*) indirect immunofluorescence. Haploid RS453 cells transformed with a 2-μm plasmid carrying *MLP1* and *MLP2-GFP* were processed for both *in situ* poly(A)$^+$ RNA hybridization and indirect immunofluorescence using anti-Nsp1p and anti-Nop1p antibodies; *a* and *e*, anti-Nsp1p staining; *b* and *f*, poly(A)$^+$ RNA staining; *c* and *g*, DNA staining with DAPI; *d*, Nomarski picture; h, merged pictures from *e, f*, and *g*. Pictures in *B* and *C* were colored and merged by digital image processing using the software program "Openlab" (Improvision, Coventry, United Kingdom).

source. When Seh1p-ProtA was affinity purified under similar conditions from 0.1% glutaraldehyde fixed spheroplasts, the 160-kDa Mlp2p band was completely absent. This result argues against an unspecific binding of Mlp2 to any nucleoporin since the Nup84p complex is located at the cytoplasmic periphery of the NPC,[3] which should not be in physical contact with the NPC-attached intranuclear filaments. In conclusion, mild glutaraldehyde fixation somehow stabilizes interaction between Nic96p and Mlp2p, allowing co-purification of Mlp2p. This agrees well with the immuno-EM data which showed that Mlp2p-ProtA is in close vicinity to the nuclear basket. Previous findings demonstrated that a pool of Nic96p is located at the terminal ring of the nuclear basket (40), where it would be expected if it functions as docking protein for the Tpr-containing filaments. Accordingly, Nic96p could serve as an NPC-attachment site for Mlp2p. However, it is possible that Nic96p is more dynamic at the NPC as recently suggested for vertebrate Nup153 (62), and Mlp2p provides an anchoring site for Nic96p on the nuclear basket of the NPC. Whether Mlp1p also interacts with Nic96p is not known, but interestingly Mlp1p-ProtA is less close to the nuclear basket than Mlp2-ProtA.

Since no heterodimer formation between Mlp1p and Mpl2p was observed, these coiled-coil proteins may be monomers or homodimers. However, more work is required to address this adequately. In an attempt to obtain a first glimpse of the structure of the yeast Tpr proteins, Mlp1p was purified and analyzed by electron microscopy after glycerol spraying/low-angle rotary metal shadowing. This revealed that Mlp1p is a thin, mostly curved filamentous molecule with a length in excess of 100 nm. Although biochemically pure, morphologically the sample appeared rather heterogeneous with only about 10% of the particles exhibiting an elongated structure. The reason for this behavior is not known, but the long and thin Mlp1p molecules may have a tendency to break during purification and/or spraying, and bend, kink, or fold back during specimen preparation. As both Mlp2p and Mlp1p harbor a long heptad-repeat containing NH_2-terminal domain, they may dimerize to form a parallel 2-stranded α-helical coiled-coil domain, thus giving the molecules their long filamentous appearance.

Do Mlp1p and Mlp2p perform an overlapping function in yeast? Although both proteins exhibit a strong homology, they do not overlap *in vivo* in a synthetically lethal relationship. One possibility is that both have a redundant role in optimizing nucleocytoplasmic transport reactions, *e.g.* in nuclear protein import (56) and mRNA export from intranuclear sites to the nuclear pores. Mlp1p and Mlp2p may have additional roles, *e.g.* in intranuclear organization or linking intranuclear structures such as peripheral chromatin or chromatin-associated proteins to the nuclear envelope and/or nuclear pores. It has been shown by immunoelectron microscopy that chromatin directly contacts the NPC-attached intranuclear filaments (63). Interesting in this context is the increased sensitivity of the *mlp1/mlp2* double disruption mutant to UV light. In *Saccharomyces cerevisiae*, telomeric chromatin is associated with the nuclear envelope; SIR proteins and Rap1p play an important role in the segregation of telomeric heterochromatin to the nuclear envelope (64). Recently, it was found that cells lacking the chromatin assembly factor-I exhibit an increased ultraviolet radiation sensitivity and reduction of telomeric silencing (65). Thus, chromatin assembly and organization with respect to telomeric silencing and DNA repair are processes in yeast that appear to require the nuclear periphery.

The C-domains of both Mlp2p and Mlp1p contain, like their higher eukaryotic counterparts (39, 59), nuclear targeting signals. In the case of Mlp2p, we could identify a short sequence at the COOH-terminal end that not only resembles a basic bipartite NLS, but binds cooperatively *in vitro* to the karyopherin α/β complex and mediates nuclear accumulation of a GFP reporter protein. Thus, the observed interaction between Mlp2p and karyopherin α/β may be used for nuclear uptake of Mlp2p. Since the C-domain of Mlp2p contains one F*X*FG motif and an extended sequence with moderate resemblance to degenerate repeat domains of classical nucleoporins, it is possible that the C-domain of Mlp2p directly interacts with karyopherin β and other β-like transport factors. However, the significance of this FSFG motif within Mlp2p remains to be shown. In any case, the C-domains of Mlp2p and Mlp1p appear to extend from the predicted filament-forming N-domain and therefore should be accessible to bind to transport factors.

Although nuclear mRNA export is not inhibited in *mlp1*$^-$ or *mlp2*$^-$ cells, overproduction of Mlp1p causes poly(A)$^+$ RNA accumulation inside the nucleus. Interestingly, mRNA accumulates in a distinct area of the nucleus which is devoid of chromatin and is neither the nucleolar compartment. Since overproduction of Mlp1p causes formation of intranuclear aggregates, it is possible that mRNPs get trapped in these Mlp1p-containing intranuclear structures. It has been shown recently

[3] B. Fahrenkrog and U. Aebi, unpublished results.

that overproduction of Mlp1p causes an extensive electron-dense fibrillogranular network, which extends from the nuclear envelope toward the nuclear interior and is highly permeable, even for large macromolecules (56). It is thus possible that mRNPs together with transport factors become trapped within these Mlp1p aggregates. Interesting in this context we found an association of Mlp2p with the Mex67p/Mtr2p mRNA exporter complex under conditions of dominant-negative RanGTP expression.[4] It is possible that this interaction represents a translocational intermediate trapped on intranuclear tracks, allowing co-isolation of Mlp2p with Mex67p/Mtr2p.

In summary, we characterized two NPC-associated proteins, Mlp2p and Mlp1p, which are the closest yeast homologues of higher eukaryotic Tpr proteins. We found that purified Nic96p is associated with a pool of Mlp2p. This implies that Nic96p (or a Nic96p complex at the terminal ring) links the yeast Tpr protein Mlp2p to the nuclear pores. Since Mlp2p can interact with protein import and nuclear mRNA export factors, and overproduction of Mlp1p inhibits mRNA export, we suggest that yeast Tpr proteins form filaments, which participate in intranuclear transport toward and away from the nuclear pores.

Acknowledgments—We are grateful to Dr. Kölling (University of Düsseldorf, Germany) for providing the *MLP1* clone, strains, and anti-Mlp1 antibodies; to Dr. M. Rexach (Stanford University, Stanford, CA) for the karyopherin α and β clones. We are also grateful to the members of our laboratory for critical reading of the manuscript.

REFERENCES

1. Ohno, M., Fornerod, M., and Mattaj, I. W. (1998) *Cell* **92,** 327–336
2. Akey, C. W., and Radermacher, M. (1993) *J. Cell Biol.* **122,** 1–19
3. Hinshaw, J. E. (1994) *Biochem. Pharmacol.* **47,** 15–20
4. Yang, Q., Rout, M. P., and Akey, Ch. W. (1998) *Mol. Cell* **1,** 223–234
5. Byrd, D. A., Sweet, D. J., Panté, N., Konstantinov, K. N., Guan, T., Saphire, A. C. S., Mitchell, P. J., Cooper, C. S., Aebi, U., and Gerace, L. (1994) *J. Cell Biol.* **127,** 1515–1526
6. Cordes, V. C., Reidenbach, S., Köhler, A., Stuurman, N., van Driel, R., and Franke, W. W. (1993) *J. Cell Biol.* **123,** 1333–1344
7. Cordes, V. C., Reidenbach, S., Rackwitz, H. R., and Franke, W. W. (1997) *J. Cell Biol.* **136,** 515–529
8. Feldherr, C. M., Kallenbach, E., and Schultz, N. (1984) *J. Cell Biol.* **99,** 2216–2222
9. Franke, W. W., and Scheer, U. (1974) in *The Cell Nucleus* (Busch, H., ed) New York
10. Gerace, L. (1986) *Trends Biochem. Sci.* **11,** 443–446
11. Goldberg, M. W., and Allen, T. D. (1992) *J. Cell Biol.* **119,** 1429–1440
12. Panté, N., and Aebi, U. (1995) *Int. Rev. Cytol.* **162,** 225–255
13. Ris, H. (1997) *Scanning* **19,** 368–375
14. Daneholt, B. (1997) *Cell* **88,** 585–588
15. Delphin, C., Guan, T., Melchior, F., and Gerace, L. (1997) *Mol. Biol. Cell* **8,** 2379–2390
16. Görlich, D., Panté, N., Kutay, U., Aebi, U., and Bischoff, F. R. (1996) *EMBO J.* **15,** 5584–5594
17. Melchior, F., Guan, T. L., Yokoyama, N., Nishimoto, T., and Gerace, L. (1995) *J. Cell Biol.* **131,** 571–581
18. Panté, N., and Aebi, U. (1996) *Science* **273,** 1729–1732
19. Wu, J., Matunis, M. J., Kraemer, D., Blobel, G., and Coutavas, E. (1995) *J. Biol. Chem.* **270,** 14209–14213
20. Wilken, N., Senécal, J. L., Scheer, U., and Dabauvalle, M. C. (1995) *Eur. J. Cell Biol.* **68,** 211–219
21. Yokoyama, N., Hayashi, N., Seki, T., Panté, N., Ohba, T., Nishii, K., Kuma, K., Hayashida, T., Miyata, T., Aebi, U., Fukui, M., and Nishimoto, T. (1995) *Nature* **376,** 184–188
22. Shah, S., Tugendreich, S., and Forbes, D. (1998) *J. Cell Biol.* **141,** 31–49
23. Franke, W. W., and Scheer, U. (1970) *J. Ultrastruct. Res.* **30,** 288–316
24. Ris, H. (1989) *Inst. Phys. Conf. Ser.* **98,** 657–662
25. Ris, H., and Malecki, M. (1993) *J. Struct. Biol.* **111,** 148–157
26. Goldberg, M. W., and Allen, T. D. (1995) *Curr. Opin. Cell Biol.* **7,** 301–309
27. Blobel, G. (1985) *Proc. Natl. Acad. Sci. U. S. A.* **82,** 8527–8529
28. Jackson, D. A., and Cook, P. R. (1988) *EMBO J.* **7,** 3667–3677
29. Beven, A., Guan, Y., Peart, J., Cooper, C., and Shaw, P. (1991) *J. Cell Sci.* **98,** 293–302
30. Kallajoki, M., Weber, K., and Osborn, M. (1991) *EMBO J.* **10,** 3351–3362
31. Nakayasu, H., and Berezney, R. (1991) *Proc. Natl. Acad. Sci. U. S. A.* **88,** 10312–10316
32. Georgatos, S. D. (1994) *J. Cell. Biochem.* **55,** 69–76
33. Gueth-Hallonet, C., Weber, K., and Osborn, M. (1997) *Exp. Cell Res.* **233,** 21–24
34. Merdes, A., and Cleveland, D. W. (1998) *J. Cell Sci.* **111,** 71–79
35. Clubb, B. H., and Locke, M. (1998) *J. Cell. Biochem.* **70,** 240–251
36. Gueth-Hallonet, C., Wang, J., Harborth, J., Weber, K., and Osborn, M. (1998) *Exp. Cell Res.* **243,** 434–452
37. Zimowska, G., Aris, J. P., and Paddy, M. R. (1997) *J. Cell Sci.* **110,** 927–944
38. Paddy, M. R. (1998) *Am. J. Hum. Genet.* **63,** 305–310
39. Bangs, P., Burke, B., Powers, C., Craig, R., Purohit, A., and Doxsey, S. (1998) *J. Cell Biol.* **143,** 1801–1812
40. Fahrenkrog, B., Hurt, E. C., Aebi, U., and Panté, N. (1998) *J. Cell Biol.* **143,** 577–588
41. Grandi, P., Schlaich, N., Tekotte, H., and Hurt, E. C. (1995) *EMBO J.* **14,** 76–87
42. Grandi, P., Emig, S., Weise, C., Hucho, F., Pohl, T., and Hurt, E. C. (1995) *J. Cell Biol.* **130,** 1263–1273
43. Belgareh, N., Snay-Hodge, S., Pasteau, F., Dahger, S., Cole, C., and Doye, V. (1998) *Mol. Biol. Cell* **9,** 3475–3492
44. Hurwitz, M. E., Strambio-de-Castillia, C., and Blobel, G. (1998) *Proc. Natl. Acad. Sci. U. S. A.* **95,** 11241–11245
45. Kölling, R., Nguyen, T., Chen, E. Y., and Botstein, D. (1993) *Mol. Gen. Genet.* **237,** 359–369
46. Sherman, F. (1990) *Methods Enzymol.* **194,** 3–20
47. Maniatis, T., Fritsch, E. T., and Sambrook, J. (1982) *Molecular Cloning: A Laboratory Manual*, Cold Spring Harbor Laboratory Press, Cold Spring Harbor, NY
48. Rothstein, R. (1983) *Methods Enzymol.* **101,** 202–211
49. Santos-Rosa, H., Moreno, H., Simos, G., Segref, A., Fahrenkrog, B., Panté, N., and Hurt, E. (1998) *Mol. Cell. Biol.* **18,** 6826–6838
50. Shevchenko, A., Jensen, O. N., Podtelejnikov, A. V., Sagliocco, F., Wilm, M., Vorm, O., Mortensen, P., Shevchenko, A., Boucherie, H., and Mann, M. (1996) *Proc. Natl. Acad. Sci. U. S. A.* **93,** 14440–14445
51. Jensen, O. N., Podtelejnikov, A., and Mann, M. (1996) *Rapid Commun. Mass. Spectrom.* **19,** 1371–1378
52. Rexach, M., and Blobel, G. (1995) *Cell* **83,** 683–692
53. Künzler, M., and Hurt, E. C. (1998) *FEBS Lett.* **433,** 185–190
54. Häner, M., Bremer, A., and Aebi, U. (1997) in *Cell Biology: A Laboratory Hand Book* (Celis, J. E., ed), 2nd Ed., Vol. 3, pp. 292–298, Academic Press, San Diego, CA
55. Segref, A., Sharma, K., Doye, V., Hellwig, A., Huber, J., Lührmann, R., and Hurt, E. C. (1997) *EMBO J.* **16,** 3256–3271
56. Strambio-de-Castillia, C., Blobel, G., and Rout, M. P. (1999) *J. Cell Biol.* **144,** 839–855
57. Siniossoglou, S., Wimmer, C., Rieger, M., Doye, V., Tekotte, H., Weise, C., Emig, S., Segref, A., and Hurt, E. C. (1996) *Cell* **84,** 265–275
58. Bailer, S. M., Siniossoglou, S., Podtelejnikov, A. V., Hellwig, A., Mann, M., and Hurt, E. C. (1998) *EMBO J.* **17,** 1107–1119
59. Cordes, V. C., Hase, M. E., and Müller, L. (1998) *Exp. Cell Exp. Cell Res.* **245,** 43–56
60. Senger, B., Simos, G., Bischoff, F. R., Podtelejnikov, A. V., Mann, M., and Hurt, E. C. (1998) *EMBO J.* **17,** 2196–2207
61. Hampsey, M. (1997) *Yeast* **13,** 1099–1133
62. Nakielny, S., Shaikh, S., Burke, B., and Dreyfuss, G. (1999) *EMBO J.* **18,** 1982–1995
63. Arlucea, J., Andrade, R., Alonso, R., and Aréchaga, J. (1998) *J. Struct. Biol.* **124,** 51–58
64. Kennedy, B. K., Gotta, M., Sinclair, D. A., Mills, K., McNabb, D. S., Murthy, M., Pak, S. M., Laroche, T., Gasser, S. M., and Guarente, L. (1997) *Cell* **89,** 381–391
65. Kaufman, P. D., Kobayashi, R., and Stillman, B. (1997) *Genes Dev.* **11,** 345–357

[4] H. Santos-Rosa and E. Hurt, unpublished results.